INTERNATIONAL JOURNAL FOR NUMERICAL METHODS IN FLUIDS
Int. J. Numer. Meth. Fluids 2001; **37**: 125–148 (DOI: 10.1002/fld.166)

Numerical simulation of mold filling in injection molding using a three-dimensional finite volume approach

Rong-Yeu Chang*,[1] and Wen-Hsien Yang[2]

Department of Chemical Engineering, National Tsing Hua University, Hsinchu, Taiwan, Republic of China

SUMMARY

This work presents an implicit finite volume approach to simulate the three-dimensional mold filling problems encountered during the injection molding. The described numerical model deals with the three-dimensional isothermal flow of incompressible, high-viscous Newtonian fluids with moving interfaces. The collocated finite volume method and the SIMPLE segregated algorithm are used to discretize and solve the Navier–Stokes equation. In addition, a bounded compressive high-resolution differencing scheme is adopted to solve the advection equation to capture the interface on a Eulerian framework. This approach effectively solves the flow field in terms of CPU time and memory storage as well as the complicated three-dimensional melt front topology. Several two- and three-dimensional examples are presented to validate the presented approach and illustrate its capabilities. This method can more accurately predict the critical three-dimensional phenomena encountered during mold filling than the existing Hele–Shaw analysis model. The presented numerical approach has been proven to be a highly effective and flexible tool for simulating mold filling problems. Copyright © 2001 John Wiley & Sons, Ltd.

KEY WORDS: finite volume method; mold filling; moving interface; three-dimensional; volume tracking

1. INTRODUCTION

Injection molding is an important industrial process for producing large quantities of complex plastic parts. New polymers and the demand for high-quality electronics, consumer products, automobiles and airplanes have forced engineers and designers to improve mold-tooling efficiency and the quality of final parts. Consequently, researchers have focused on developing an efficient analysis tool to replace the experimental trial-and-error process. Recent progress in both hardware and software has made computer-aided engineering (CAE) a highly effective tool for analysing the complicated physical phenomena inherent in the injection molding [1].

* Correspondence to: Department of Chemical Engineering, National Tsing-Hua University, Hsinchu, Taiwan 30043, Republic of China. Tel.: +886 3 5718344; fax: +886 3 5727608.
[1] E-mail: rychang@che.nthu.edu.tw
[2] E-mail: yws@che.nthu.edu.tw

Received May 2000
Revised July 2000

During the injection molding process, the polymer melt is forced to flow, under constant high pressure, through the sprue, runner and then fill into the empty cavity. The plastic part is ejected after the polymer melt is sufficiently cooled and hardened.

Over the last two decades, numerous researchers have attempted to analyse such a complex process by distinct simplifications and approximations under the limited computational resources [2–6]. The Hele–Shaw model [4] has been extensively adopted in the current commercial CAE packages. The Hele–Shaw model neglects the inertia and the gapwise velocity component for polymer melt flow in thin cavities. The flow governing equations are simplified into a single Poisson equation based on these assumptions [7]. In this manner, the requirements of the computational storage and CPU time requirements can be considerably reduced. However, such a simplified model possesses some limitations. First, the shell element employed in the Hele–Shaw model needs the construction of the mid-plane, which is time-consuming. Furthermore, some significant three-dimensional flow regions, i.e. flow around corners, over bosses, ribs or thickness-change regions, or the fountain effect in the vicinity of melt fronts, may remain in thin cavities. These regions will not only complicate the identification of the mid-plane but will also cause pressure, heat transfer or stress prediction errors. Moreover, the dominant three-dimensional flow featured in thick parts, such as gears and connectors, invalidates the Hele–Shaw approximation in these cases.

Therefore, a true three-dimensional analysis model is necessary not only to reduce the time spent in the construction of the mid-plane, but also to accurately predict the flow in the thick parts. A true three-dimensional analysis can give more insight into the microstructure of parts by providing detailed information about fiber orientation, residual stress or degree of cure distributions, etc. However, the highly non-linear interplay between transient heat transfer, non-Newtonian fluid flow, moving interface and phase change challenges the accuracy, efficiency and stability of the fully three-dimensional mold filling analysis.

The three-dimensional simulation of mold filling especially struggles to accurately calculate the polymer–air interface of complex topology and its evolution over time. Serious effort has been devoted to developing numerical models to calculate the moving interface problems over the last two decades. An extensive review of moving interface problems can be found in Reference [8]. The volume tracking (or surface capturing) methods based on a fixed mesh can efficiently model the mold filling problems due to their topological robustness and efficiency. In the volume tracking method, the interface is not explicitly tracked, but implicitly captured by cells that are partially filled. This is achieved by either following imaginary particles (marker and cell (MAC) [9]) or solving the transport equation for the fractional volume function. The latter is more economical in terms of CPU time and computer storage for three-dimensional applications. The transport equation for the fractional volume function can generally be solved by two distinct approaches: geometrical and algebraic [10]. The flow solver is performed in the filled area only in the geometrical approach. The interface must be reconstructed in each partially filled cell to accurately calculate the fluid quantities across the faces of the interface cell, and to properly impose the boundary conditions on the interface. In the earlier works of this kind approach, Hirt's volume of fluid method (VOF) [11] is perhaps the most widely adopted approach to model the two-dimensional mold filling problems [12–15]. Numerous researchers have attempted to improve the original VOF [16–19]. Recently, Rider [20] derived a reconstruction scheme of second-order accuracy both in space and

time and extended it to the unstructured mesh. Gao [21] successfully combined this scheme with the finite element method (FEM) to simulate the three-dimensional mold filling during casting process.

In the algebraic approach, the velocity field is calculated over the entire cavity domain, including the empty and filled areas. The moving interface is captured by directly solving the hyperbolic transport equation for the fractional volume function. Special care is needed to derive convection differencing schemes that maintain a sharp interface and produce monotone profiles of the fractional volume function. The algebraic approach has been employed to track the interface in mold filling simulations [22–25]. However, interface smearing remained problematic, particularly when first-order differencing schemes such as upwind are used. Recently, Ubbink [26] proposed a bounded compressive high-resolution differencing scheme to combat the numerical diffusion that occurs when solving the moving interface problems. The algebraic approach is preferred in the present work because it can perform multi-fluid modeling, such as gas-assisted or multiplayer injection molding processes, and can avoid the difficulties in imposing boundary conditions on the interface.

The finite difference method (FDM) and FEM have been extensively employed to solve moving interface problems. Although the FDM is a simple and efficient numerical method, it is restricted to regular physical domain. To overcome this restriction, the FDM is generally incorporated with the boundary fitted co-ordinate system (BFCS), which becomes complicated and impractical for complex three-dimensional geometries. The FEM has been conventionally adopted to model polymer processing because of its flexibility in dealing with arbitrary boundary shapes. However, it tends to produce a large sparse matrix, generally with high condition numbers, and as a consequence relies on the direct solvers, which becomes inefficient and needs too much computer space for a large-scale system. In the last decade, the collocated finite volume method (FVM) based on the pressure correction procedures such as the SIMPLE [27] algorithm has been developed and employed widely in conventional computational fluid dynamics (CFD) applications [28]. It has recently been formulated to be able to deal with the geometry of an arbitrary shape on an unstructured mesh framework without boundary-fitted co-ordinate transformation [29–31]. The FVM can more efficiently utilize both time and computer space and is also more computationally stable then the FEM when modeling polymer processing.

The objective of this work is to develop an efficient and robust three-dimensional FVM to model the isothermal mold filling in the injection molding. The incompressible Navier–Stokes equations are discretized via the implicit collocated FVM. To minimize storage requirements, a segregated solution strategy is favored, with pressure and velocity coupled using the SIMPLE algorithm. The melt front advancement is captured by the algebraic volume tracking method, while the fractional volume function advection equation is discretized by a bounded compressive high resolution differencing scheme. The second-order accuracy is carefully maintained both in time and space. Several examples are investigated to assess the performance of the developed method. The fountain flow in the vicinity of melt front is first studied by the presented method on a fixed mesh framework. The melt flows in three various three-dimensional thin rectangular plate cavities are then examined to compare the conventional Hele–Shaw model with the proposed three-dimensional model. Finally, the filling of a complex three-dimensional cavity is simulated to illustrate the capabilities of the presented method.

2. MATHEMATICAL MODEL

2.1. Geometry

Figure 1 illustrates an example of a simple mold cavity. In the present work, the transport equation for the fractional volume function is solved by the algebraic technique to track the melt front in the molding process. The total computational domain Ω covers both the melt and air region in the cavity, i.e. $\Omega = \Omega_{\text{melt}} \cup \Omega_{\text{air}}$. The melt and air regions are considered to be a continuous fluid of different physical properties.

2.2. Governing equations

The three-dimensional incompressible and isothermal flow is mathematically described by the conservation laws, namely the conservation of mass (continuity equations) and conservation of momentum (momentum equation). These governing equations can be cast in the conservation form as follows:

Continuity equation

$$\frac{\partial}{\partial t}\rho + \nabla \cdot \rho \mathbf{u} = 0 \tag{1}$$

Momentum equation

$$\frac{\partial}{\partial t}(\rho \mathbf{u}) + \nabla \cdot (\rho \mathbf{u}\mathbf{u} - \mathbf{T}) = \rho \mathbf{g} \tag{2}$$

where t is the time, ρ the density, $\mathbf{u}$ the velocity vector, $\rho \mathbf{g}$ the gravity force and $\mathbf{T}$ is the total stress tensor. For an incompressible Newtonian fluid, the total stress tensor $\mathbf{T}$ is defined as follows:

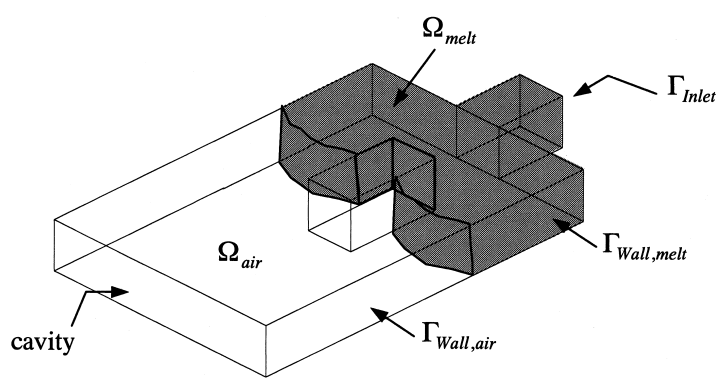

Figure 1. General description of a mold cavity.

$$\mathbf{T} = -p\mathbf{I} + 2\mu\mathbf{D} \tag{3}$$

where p is the presssure, μ the viscosity of fluid, $\mathbf{I}$ the unit tensor and $\mathbf{D}$ the rate of strain tensor

$$\mathbf{D} = \frac{1}{2}(\nabla\mathbf{u} + \nabla\mathbf{u}^T)$$

The momentum equation is closely coupled with the viscosity and density constitutive relations. The following simple serial averages are adopted in this work to approximate the viscosity and density at the interface between the melt and the air

$$\mu = f\mu_1 + (1 - f_1)\mu_2 \tag{5}$$

$$\rho = f\rho_1 + (1 - f_1)\rho_2 \tag{6}$$

where the subscripts denote the different fluids. The fractional volume function is defined as follows

$$f(\mathbf{x}, t) = \begin{cases} 1 & \text{for the point } (\mathbf{x}, t) \text{ inside fluid 1} \\ 0 & \text{for the point } (\mathbf{x}, t) \text{ inside fluid 2} \end{cases} \tag{7}$$

The fluid 1 is the melt and fluid 2 is the air. Then the interface is located within the cells where $0 < f < 1$. The fractional volume function is governed by a transport equation

$$\frac{\partial}{\partial t} f + \mathbf{u} \cdot \nabla f = 0 \tag{8}$$

This equation determines the movement of interface position.

2.3. Boundary conditions

The initial and boundary conditions for the flow domain must be defined to complete the mathematical description of the whole system. The boundary conditions are

- At the inlet gate Γ_{inlet}. A constant flow rate of polymer melt is specified at the inlet gate

$$\mathbf{u} = \mathbf{u}_{\text{specified}} \text{ on } \Gamma_{\text{inlet}} \tag{9}$$

- At the mold boundaries. The imposing of slip or no-slip boundary condition at the mold boundaries will result in the unrealistic interface predictions as encountered in the earlier research of this work. The procedure described in Reference [25] is employed to overcome this problem, i.e. no polymer melt is allowed to cross the mold walls, but the air is assumed to be free to leave the mold as the polymer melt advance. Consequently, no-slip and

traction free boundary conditions are switched dynamically according to the filling status there. The no-slip boundary condition is applied if it is filled, namely $f \geq f_c$, otherwise the traction free boundary condition is used if $f < f_c$. f_c is chosen as 0.5 in this work.

(a) For the filled mold wall (melt) $\Gamma_{\text{wall,melt}}$

$$\mathbf{u} = 0 \text{ on } \Gamma_{\text{wall,melt}} \tag{10}$$

(b) For the empty mold wall (air) $\Gamma_{\text{wall,air}}$:

$$\mathbf{T} \cdot \mathbf{n} = 0 \text{ on } \Gamma_{\text{wall,air}} \tag{11}$$

- The initial conditions. All dependent variables must be initialized first in the transient calculation.

For the first-order hyperbolic transport equation of fractional volume, only an inlet condition and an initial condition throughout the domain are necessary.

3. NUMERICAL MODEL

The FVM based on the pressure-based decoupled procedure is adopted to solve the transient flow field in complex three-dimensional geometry. Besides, a compressive bounded high-order differencing scheme is also utilized to directly solve the hyperbolic advection equation of fractional volume function to track the melt front during filling process. The details of these two methods and how to couple the velocity and interface movement will be addressed in the following subsections.

3.1. The Navier–Stokes solver

3.1.1. Finite volume discretization. The whole computational domain is subdivided into a finite number of non-overlapping control volumes or cells of arbitrary topology (see Figure 2) in the FVM. The collocated variable arrangement is used, i.e. the transport variables are stored at the centroid of the control volumes. Each internal cell face has one cell on either side. The transport equations are then integrated over each of the control volumes in the domain by approximating the distribution of dependent variables in space and time with piecewise profiles, also known as the differencing schemes.

All the above governing equations can be cast into the following generic form with appropriate choice of ϕ, Γ and Q_ϕ

$$\frac{\partial}{\partial}(\rho\phi) + \nabla \cdot (\rho \mathbf{u}\phi) - \nabla \cdot (\Gamma \nabla \phi) = Q_\phi \tag{12}$$

where ϕ denotes the dependent variable which can be a scalar or vector components, Γ is the diffusivity, and Q_ϕ is called the source term which contains all the terms that cannot be

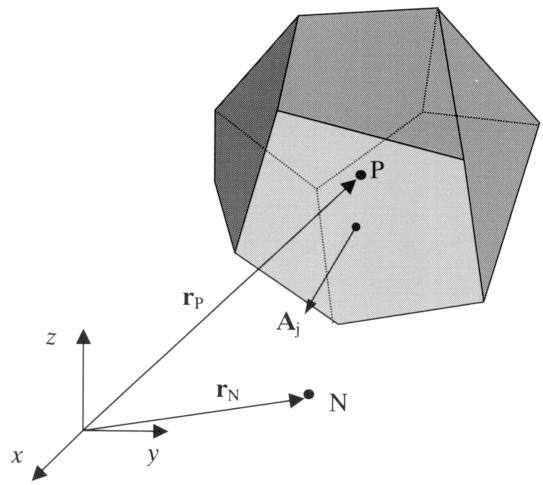

Figure 2. Illustration of a typical control volume of arbitrary topology.

accommodated in the convection and diffusion term. This equation contains four distinct parts: unsteady, convection, diffusion and source terms. All vector or tensor variables are computed in their Cartesian components, and hence no co-ordinate transformation is required, which considerably simplifies the complicated full three-dimensional primitive variables flow calculation.

Integrating this equation over the respective control volume (with volume V and bounding surface $\Sigma_{j=1}^{n} \mathbf{A}_j$) and using the Gauss divergence theorem whenever possible gives

$$\int_V \frac{\partial}{\partial t}(\rho\phi)\,\mathrm{d}V + \sum_{j=1}^{n} \int_{\mathbf{A}_j} (\rho\mathbf{u}\phi - \Gamma\nabla\phi)\cdot\mathrm{d}\mathbf{A} = \int_V Q_\phi\,\mathrm{d}V \tag{13}$$

where n is the number of cell-faces of a cell. The midpoint approximation rule is adopted to calculate the surface and volume integrals, which is of second-order accuracy and only the value of integrand at the center of face or cell is required. Equation (13) for control volume P can then be re-written as follows

$$\left(\frac{\partial\rho\phi}{\partial t}\right)_P V_P + \sum_{j=1}^{n} (\rho\phi\mathbf{u})_j \cdot \mathbf{A}_j - \sum_{j=1}^{n} (\Gamma\nabla\phi)_j \cdot \mathbf{A}_j = (Q_\phi)_P V_P \tag{14}$$

The linear interpolation is used to approximate the values of the dependent variables at cell-face centers, and then the surface integrals can be evaluated. The Gauss divergence theorem is utilized to calculate the gradient of dependent variables at the cell centers [28]. The

first-order upwind scheme is known to be extremely stable but diffusive due to the upwind effect. Therefore, the Khosla and Rubin's deferred correction scheme [32] is adopted to blend these two schemes

$$\phi_j = \phi_j^{\text{upwind}} + \gamma_\phi[\phi_j^{\text{interp}} - \phi_j^{\text{upwind}}]^{\text{old}} \tag{15}$$

where γ_ϕ is the blending factor with a value between zero and one. The term in brackets is treated explicitly. Therefore, the stable computation is achieved during iteration while solution of second-order accuracy is obtained when converged. The Equation (16) proposed by Muzaferija [29] is adopted herein to approximate the gradient of dependent variables at the cell-face centers while evaluating the surface integral of diffusion term on a non-orthogonal grid

$$(\nabla\phi)_j = \overline{(\nabla\phi)}_j + \left(\frac{\phi_N - \phi_P}{|\mathbf{r}_N - \mathbf{r}_P|} - \overline{(\nabla\phi)}_j \cdot \frac{\mathbf{r}_N - \mathbf{r}_P}{|\mathbf{r}_N - \mathbf{r}_P|}\right)\frac{\mathbf{A}_j}{|\mathbf{A}_j|} \tag{16}$$

where the value of $\overline{(\nabla\phi)}_j$ is calculated by linear interpolation between control volume P and its neighbor N and $\mathbf{r}$ is the position vector. The three-time levels implicit Euler scheme is chosen for temporal differencing in light of its second-order temporal accuracy and the feasibility of larger time step size.

After summing all the terms featuring in Equation (14), the final algebraic equation which links the value of the dependent variable at the cell center with the neighboring values can be written as follows:

$$\mathbf{A}\boldsymbol{\varphi} = \mathbf{b} \tag{17}$$

where $\mathbf{A}$ is a matrix, which is sparse and diagonal-dominated, resulting from the aforementioned discretization, $\boldsymbol{\varphi}$ is the solution vector, and $\mathbf{b}$ is the vector source term. The iterative methods are used to solve the discretized algebraic equations. A very efficient conjugate gradient (CG) method is employed herein when matrix $\mathbf{A}$ is symmetric and the BiCGSTAB method when matrix $\boldsymbol{A}$ is asymmetric, both preconditioned with an incomplete LU decomposition (ILU) preconditioner [33].

3.1.2. Discretized momentum equation. In the same manner as described above, the momentum equation can be discretized

$$a_P u_P^i + \sum_{nb} a_{nb} u_{nb}^i = b_P^i \tag{18}$$

The summation is over all the neighbors of cell P. u^i is the Cartesian component of the velocity vector. a_{nb} contains contributions from surface integrals over faces common to the cell around the computational node P and the corresponding neighbors. a_p contains in addition contributions from the unsteady term and possibly from volume integrals. The source term b_P^i contains the pressure gradient, components of the stress tensor not included in the standard diffusion term and also the explicit part of the deferred correction scheme.

3.1.3. Calculation of pressure. Some special means needs to be devised to compute the pressure field for incompressible flows since no explicit equation exists for the pressure field. A procedure similar to the SIMPLE algorithm is employed in this work. The procedure is briefed below. The discretized form of the continuity equation for each control volume can be written as

$$\sum_{j=1}^{n} \mathbf{u}_j \cdot \mathbf{A}_j = 0 \tag{19}$$

Special care is required to avoid the possible decoupling of the velocity and pressure while computing the face volume fluxes in the calculation of pressure on a collocated variable arrangement. The momentum interpolation proposed by Rhie and Chow [34] is adopted to evaluate the face volume fluxes

$$\mathbf{u}_j^* = \overline{\mathbf{u}_j^*} - \overline{\left(\frac{V}{a_P}\right)}_j \left[\frac{p_N - p_P}{|\mathbf{r}_N - \mathbf{r}_P|} - \frac{\overline{(\nabla p)}_j \cdot (\mathbf{r}_N - \mathbf{r}_P)}{|\mathbf{r}_N - \mathbf{r}_P|}\right] \tag{20}$$

where * denotes the temporary new value obtained from the discretized momentum equation, the over bar means an arithmetic average between control volumes adjacent to the cell face j. The above equation representing a face cell velocity equals a linear interpolation of the cell-center velocities plus a correction involving a third-order pressure gradient term, which senses the unphysical oscillation in pressure solution and smoothes it. The SIMPLE algorithm introduces the pressure correction p' to correct the volume fluxes $J_i^* = (\mathbf{u}^* \cdot \mathbf{A})_j$ calculated above to satisfy the continuity equation

$$\sum_{j=1}^{n} (J_j^* + J_j') = 0 \tag{21}$$

where the correction J_f' is defined as

$$J_j' \approx -\overline{\left(\frac{V}{a_P}\right)}_j \left(\frac{p_N' - p_P'}{|\mathbf{r}_N - \mathbf{r}_P|}\right) |\mathbf{A}_j| \tag{22}$$

Substituting Equation (22) into Equation (21) yields the pressure-correction equation of the same form as Equation (18). The semi-implicitly procedure described in Reference [28] can be utilized to improve the convergence for the extremely non-orthogonal grids.

3.1.4. Solution procedure for flow field. The SIMPLE is an iterative decoupled procedure for coupling velocity and pressure, in which the three linearized momentum equations are solved for a guessed pressure field, sequentially followed by solution of the pressure correction equation. The mass fluxes and pressure are then corrected. This will satisfy both local and global continuity but deviate momentum conservation. Hence, a new outer iteration is activated. The process is repeated until the prescribed tolerance for each equation is achieved. A drop in the residual level of four orders of magnitude is considered to converge in this work.

3.2. Melt–air front tracking algorithm

As mentioned in the introduction, a fractional volume function is used to track the moving interface. After the velocity field has been calculated at each time step, we need to solve the fractional volume advection equation from the given velocity field to determine the new position of the interface. The fractional volume advection equation is hyperbolic in nature and with discontinuity on the melt–air interface. Consequently, special care is required to solve this advection equation with minimum diffusion to preserve the sharpness of the interface.

Substituting the continuity equation, $\nabla \cdot \mathbf{u} = 0$, into Equation (8), we obtain

$$\frac{\partial}{\partial t} f + \nabla \cdot f\mathbf{u} = 0 \tag{23}$$

Following the similar finite volume procedure described above and applying Crank–Nicolson scheme, Equation (23) can be discretized over control volume P as

$$f_P^{t+\Delta t} = f_P^t + \frac{\Delta t}{V_P} \sum_{j=1}^{n} (f_j^* \mathbf{u}_j \cdot \mathbf{A}_j) \tag{24}$$

The variation of volume flux within Δt time interval is neglected for saving computational efforts. f_j^* is the time averaged value of face volume flux within Δt time interval

$$f_j^* = \frac{1}{2} (f_j^{t+\Delta t} + f_j^t) \tag{25}$$

f is like a step function that separates the fluid region from the empty region. Applying the conventional spatial interpolation scheme to approximate the face fractional volume function f_j will introduce too much numerical diffusion and hence smear the sharp interface [19]. To overcome this problem, many different differencing schemes have been proposed with attempts to minimize the numerical diffusion [10]. However, none can give a promising solution, either too diffusive or unbounded. Recently, Ubbink *et al.* [26], based on the normalized variable diagram (NVD) [35], proposed a compressive bounded high-resolution scheme, named the compressive interface capturing scheme for arbitrary meshes (CICSAM), to deal with contact discontinuities such as fluid interfaces, and extended it to unstructured meshes. The CICSAM applies the NVD to ensure the boundness in approximating the face volume fluxes, and switches between two different high-resolution schemes to insure the sharpness of the interface. An outline of the CICSAM is given below to facilitate the understanding of its theoretical background. Refer to Reference [26] for the details.

The normalized variable of f is defined as

$$\tilde{f} = \frac{f - f_U}{f_A - f_U} \tag{26}$$

where the subscript D denotes the donor cell, A the acceptor cell and U the upwind cell. The upper bound of the convection boundness criterion (CBC) described in Equation (27) is the most compressive differencing scheme because it converts all gentle gradients into sharp steps, as indicated by Leonard and named as the Hyper-C [35].

$$\tilde{f}_{j\mathrm{CBC}} = \begin{cases} \min\left\{1, \dfrac{\tilde{f}_D}{c}\right\} & \text{for } 0 \le \tilde{f}_{\mathrm{D}} \le 1 \\ \tilde{f}_{\mathrm{D}} & \text{for } \tilde{f}_{\mathrm{D}} < 0 \text{ or } \tilde{f}_{\mathrm{D}} > 1 \end{cases} \tag{27}$$

where $c = \Sigma_{j=1}^{n} |c_f^{\mathrm{out}}|$ is the Courant number of the donor cell. Such a characteristic is desired in the current modeling of moving interface problems. However, it is unstable due to its tendency to wrinkle the interface when the orientation of interface is normal to the flow direction [19]. In light of this, the ULTIMATE–QUICKTEST (UQ) [35] described below is adopted in the CICSAM to continue the calculation where the Hyper-C is inadequate

$$\tilde{f}_{j\mathrm{UQ}} = \begin{cases} \min\left\{\dfrac{8c\tilde{f}_{\mathrm{D}} + (1-c)(6\tilde{f}_{\mathrm{D}} + 3)}{8}, \tilde{f}_{j\mathrm{CBC}}\right\} & \text{for } 0 \le \tilde{f}_{\mathrm{D}} \le 1 \\ \tilde{f}_{\mathrm{D}} & \text{for } \tilde{f}_{\mathrm{D}} < 0 \text{ or } \tilde{f}_{\mathrm{D}} > 1 \end{cases} \tag{28}$$

The UQ is a high-resolution differencing scheme but it is still too diffusive to apply anywhere in the calculation of moving interface problems. Consequently, depending upon the orientation of the interface, the CISCAM applies a weighting factor $1 \le \gamma_j \le 0$ to smoothly switch between these two methods

$$\tilde{f}_j = \gamma_j \tilde{f}_{j\mathrm{CBC}} + (1 - \gamma_j)\tilde{f}_{j\mathrm{UQ}} \tag{29}$$

where γ_j is related to the angle between the interface orientation and flow direction [26]. The fractional volume function on the cell face can then be obtained by rearranging Equation (29) according to Equation (26). This is the basis of the CICSAM formulation of cell-face values for one-dimensional flow. For more details concerning the extension to multi-dimensions and unstructured meshes the reader is referred to Reference [26].

After solving the Navier–Stokes equations as described above, the interface advancement at each time step is determined by solving the fractional volume advection equation according to the velocities obtained. The interface is coincident with the contour of $f = 0.5$. Both the flow solver and the interface advection are solved implicitly by the second-order scheme. Consequently, a larger time step size can be used in the transient calculation and hence reduce the total number of time steps. This will result in a substantial speed-up in the flow calculation and will also increase the overall efficiency. Of course, the use of Courant numbers greater than one introduces non-negligible numerical diffusion of the conveyed function f but it offers a trade-off between accuracy and computational time. A Courant number of $c = 0.5$ will be used in the present work.

4. NUMERICAL RESULTS

Extensive calculations were performed for several two- and three-dimensional examples to assess the accuracy, efficiency and robustness of the proposed numerical model.

4.1. Fountain flow

The fountain flow is located near the advancing melt front in the injection molding. It is important because it significantly influences the microstructure of the molded parts such as the fiber orientation and residual stress or degree of cure distributions. However, the fountain effect is ignored in the Hele–Shaw approximation. The accuracy of the presented numerical model was verified by simulating the fountain flow in the injection molding.

The computational domain is confined to the rectangular region between two parallel plates, while the material properties of the polymer melt and the air are as follows: $\mu_{\text{melt}} = 2000.0$ g cm^{-1} s^{-1}, $\mu_{\text{air}} = 1.0$ g cm^{-1} s^{-1}, $\rho_{\text{melt}} = 1.0$ g cm^{-3}, $\rho_{\text{air}} = 1.23 \times 10^{-3}$ g cm^{-3}. Since the air velocity and pressure are not of great interest, the air viscosity is slightly increased to enhance the solution convergence. Figure 3 shows the evolution of the predicted position of the melt–air interface at different times. The following parameters are defined according to the experiment data obtained by Behrens [36] to make a quantitative comparison: x_{FT} is the flow-tip of the current front, x_{CL} denotes the position of the contact line and h represents the gapwise thickness. The predicted results are compared against experimentally derived values in Figure 4. The contact point is not moved but overrode by the advancing front element instead as a result of the fountain effect as illustrated by the velocity vectors and the melt streamlines in Figure 5. Imposing artificially the no-slip or partially slip boundary conditions at this triple point (melt–air–solid) will result in inaccurate predictions of the melt front shape and its positions. This problem is remedied herein by dynamically adjusting the wall boundary conditions according to the movement of the melt front. This approach is justified by the close

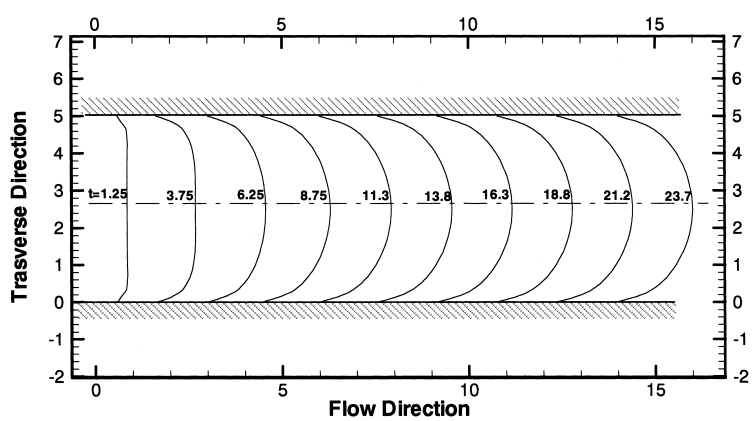

Figure 3. Evolution of flow front shape.

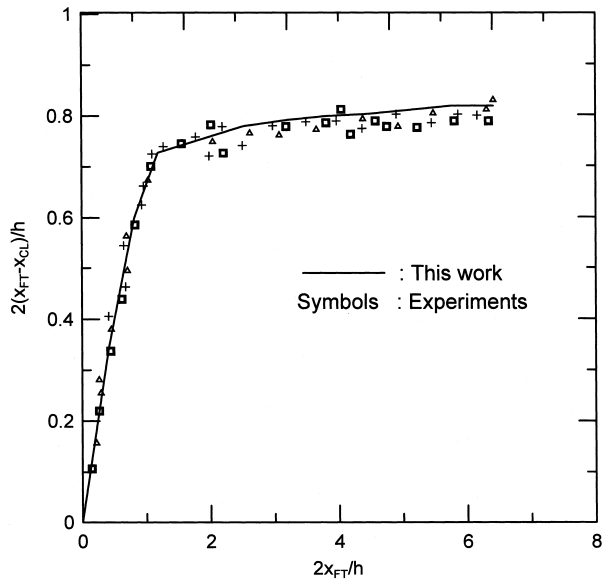

Figure 4. Calculated and experimental front development.

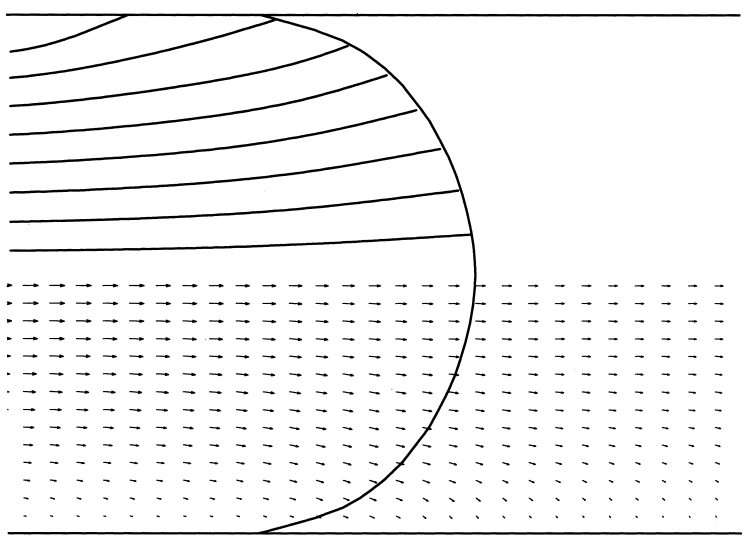

Figure 5. Calculated velocity vectors and streamlines of melt.

correlation between the numerical and experimental reults. Figure 6 displays the flooded contour plot of the fractional volume function. The developed model can properly control the numerical diffusion within one to two cells, and hence preserve a sharp interface as desired.

4.2. Three-dimensional mold filling studies

Three numerical examples were simulated in this subsection to compare the Hele–Shaw approximation with the true three-dimensional analysis. The Hele–Shaw model analysis results were obtained by Moldex [37]. The material properties of the polymer melt and the air are the same as those in Subsection 4.1. The filling time for all three cases is chosen as 2.0 s.

The first example is of a three-dimensional thin rectangular mold filling a cavity of $15 \times 10 \times 0.2$ cm. A point gate is located at the right end side center of the mold as illustrated in Figure 7. The total CV number is 5840 and the gapwise direction is divided into eight CVs. Figure 8 compares the simulated melt fronts obtained by the Hele–Shaw model and the three-dimensional model. The predicted mold filling patterns are virtually identical for this thin rectangular cavity. The three-dimensional model predicts a curved melt front in the gapwise direction due to the fountain effect near the melt front. The fountain effect region (the distance between the tip and contact point) in the above fountain flow study is approximately the same order of magnitude as the the thickness of cavity according to Figure 4. In contrast, the Hele–Shaw model ignored the fountain effect and assumed a flat front profile in the gapwise direction. The predicted inlet-pressure profile versus filling time is presented in Figure 9. The Hele–Shaw and the presented three-dimensional model created identical inlet pressure profiles.

The second case is to illustrate the capability of the present three-dimensional model to deal with the splitting and remerging of the melt fronts during the filling process, and make a further validation by comparing with the Hele–Shaw model. The geometry, displayed in Figure 10, is obtained by coreing out a small rectangular volume in the cavity of the first example. The cavity is meshed with 6288 CVs. Figures 11 and 12 compare the melt fronts and inlet pressure profiles obtained from both models respectively. As expected, the predictions of both models correlate with each other. It is noted that the Hele–Shaw model predictes a slightly faster melt front advancement in the vicinity of the side mold walls than the three-dimensional model because of the slip boundary assumption inherent in the Hele–Shaw model.

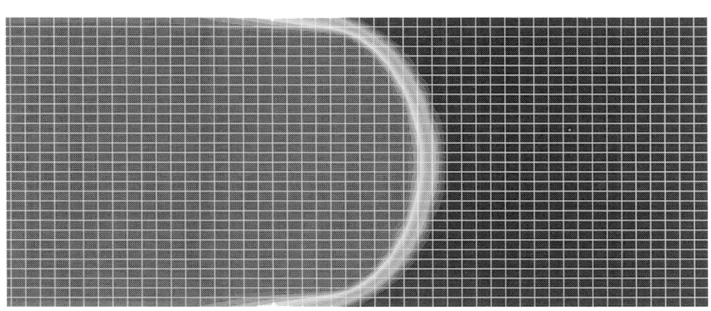

Figure 6. Flooded contour plot of fractional volume function.

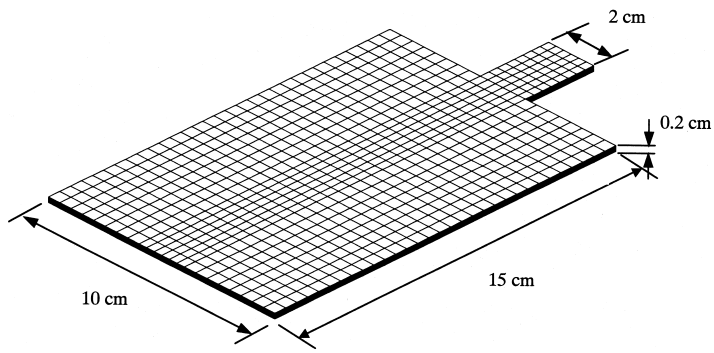

Figure 7. Numerical mesh for the rectangular plate example 1.

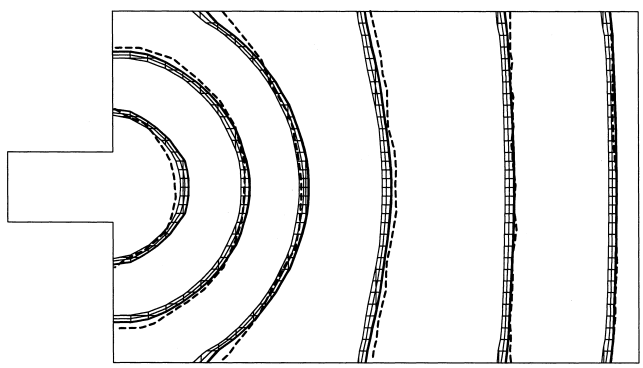

Figure 8. Comparison of the simulated melt fronts from the Hele–Shaw and the three-dimensional models for example 1 (dashed line, 2.5D; meshed surface, 3D).

To examine the influence of the mesh density on the predicted results, the flow regions above and below the cored volume are meshed with two different element sizes. Figure 13 shows the postions of the melt front at several distinct time steps in this area. The flow symmetry appears to be well predicted and mesh independent. The shapes of the melt front are also properly represented except that the predicted interfaces are sharper in the region with fine mesh than those in the coarse mesh.

Since the above two cavities are thin in thickness compared with the planar dimensions, the Hele–Shaw model can produce accurate predictions for these two examples as confirmed by the three-dimensional model. The developed three-dimensional model was also tested for a situation where the Hele–Shaw approximation does not function very well: the same geometry as the first example except that the cavity is significantly thicker in the left region. The thickness in this region is increased from 2 to 6 mm, as displayed in Figure 14. The mesh

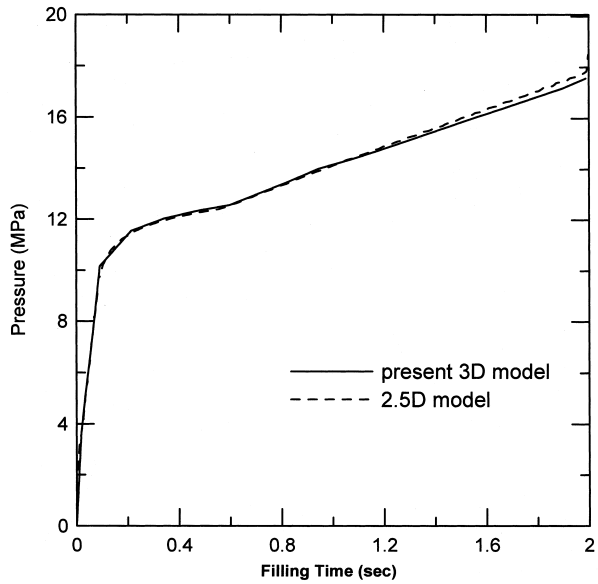

Figure 9. Comparison of the simulated filling pressures from the Hele–Shaw and the three-dimensional models for example 1.

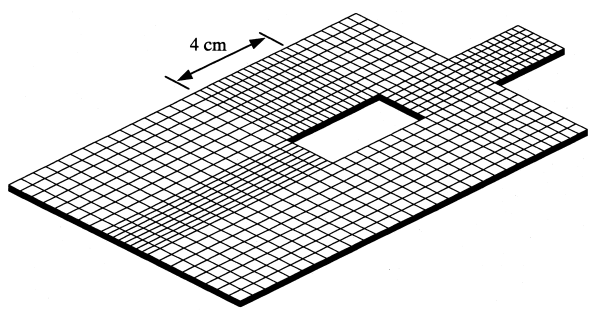

Figure 10. Numerical mesh for the rectangular plate example 2.

employed for the filling analysis contains 8448 CVs. The gapwise directions of the thin and thick regions are meshed with eight and 16 CVs respectively. The steep thickness change in this case will result in significant three-dimensional flow phenomena there. Figure 15 compares the predicted filling patterns from both Hele–Shaw and three-dimensional models at several distinct times. The velocity vectors predicted by the three-dimensional model are also displayed in this figure. Although the predicted melt front reveals similar trends for both models, the correlation is not as good as in the above two examples, particularly in the radial flow region.

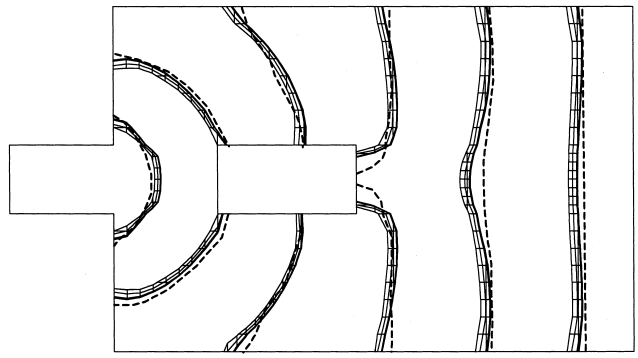

Figure 11. Comparison of the simulated melt fronts from the Hele–Shaw and the three-dimensional models for example 2 (dashed line, 2.5D; meshed surface, 3D).

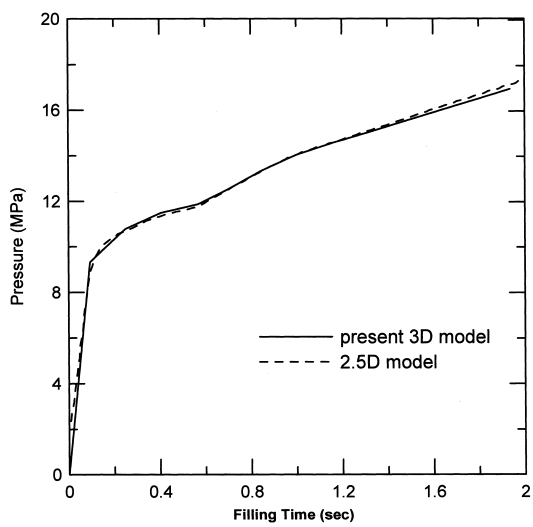

Figure 12. Comparison of the simulated filling pressures from the Hele–Shaw and the three-dimensional models for example 2.

The melt advances from the thin region into the thick region in the radial flow region, resulting in an obvious gapwise velocity component. Consequently, the melt must move upward until it reaches the top mold wall in addition to advancing forward in the planar direction, which will take some time. This phenomenon is captured in the developed three-dimensional model as indicated in Figure 16, where the shadings of the melt fronts are plotted by viewing from the gating direction. In contrast, the Hele–Shaw model neglects the gapwise velocity component

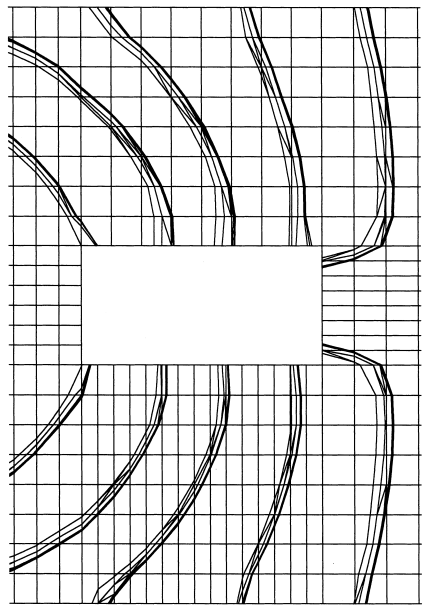

Figure 13. Effect of mesh density on the predition of the melt front.

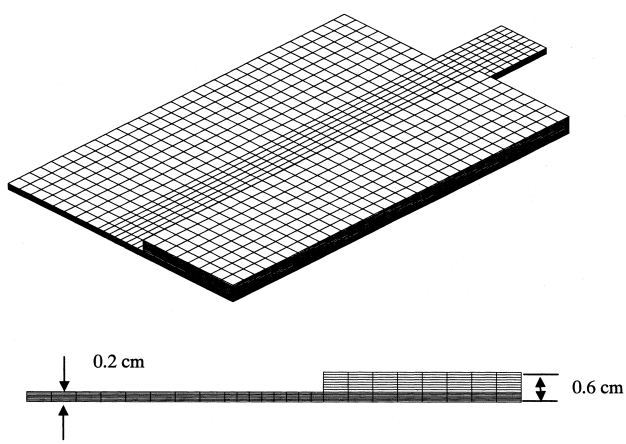

Figure 14. Numerical mesh for the rectangular plate example 3.

and assumes that the melt can immediately fill the complete cross-section of the region that it reaches. Consequently, in this case, the Hele–Shaw model predicts an always faster front advancement in the thick region than that in the thin region, where the flow resistance is

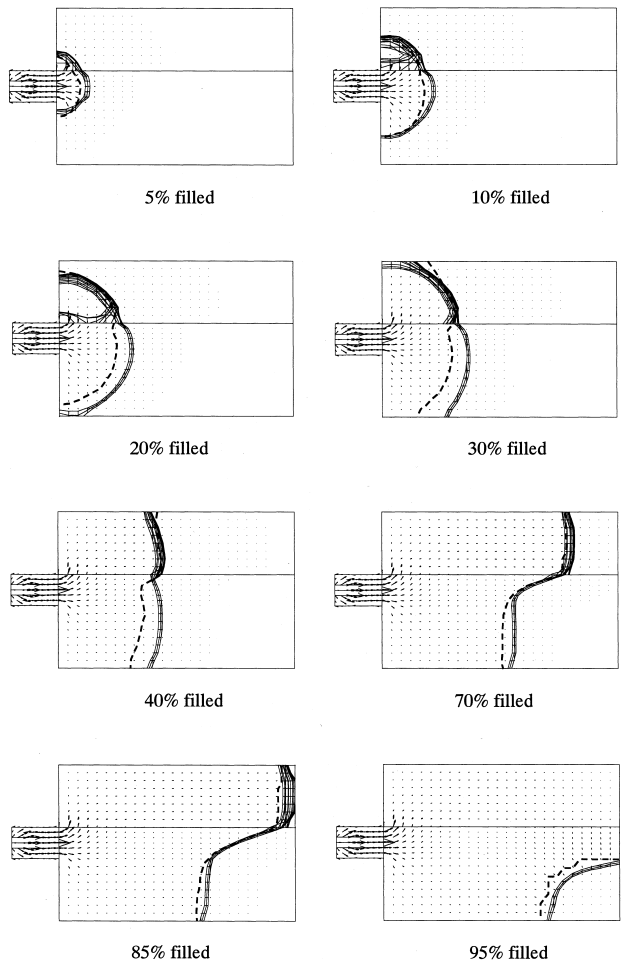

Figure 15. Comparison of the simulated melt fronts from the Hele–Shaw and the three-dimensional models for example 3 (dashed line, 2.5D; meshed surface, 3D).

relatively larger. Alternatively, the described three-dimensional model predicts a slower melt advancement in the radial flow region of the thick cavity due to the aforementioned three-dimensional effect. Additionally, Figure 16 also indicates that the formation of a circulation area is predicted in the upper right corner of the thick region. The discrepancy in the predicted melt front positions is reduced after the cavity is half filled because of the dominant parallel filling patterns in the planar direction, and hence the melt starts to move faster in the thick region than in the thin region. Figure 17 compares the inlet pressure profiles obtained from both models. The predicted inlet pressure profiles from both models disagree in the radial flow region due to the significant three-dimensional flow. However, the Hele–Shaw

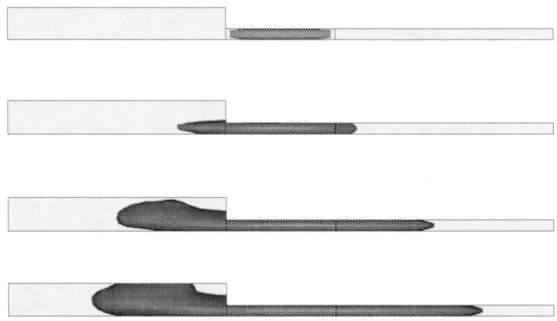

Figure 16. Simulated melt fronts by viewing from gating direction.

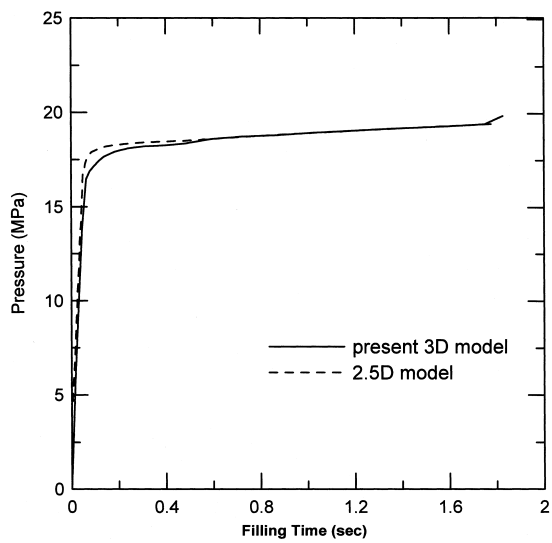

Figure 17. Comparison of the simulated filling pressures from the Hele–Shaw and the three-dimensional models for example 3.

model can still provide an essentially identical inlet pressure prediction with the three-dimensional model in this case as a whole.

4.3. Filling simulation of a gear part

In order to demonstrate our model in a complex geometry, the filling of a gear mold was simulated. The computational mesh utilized for this example was comprised of 8000 CVs, as presented in Figure 18. The mold was filled with two gates located at the two diagonal corners

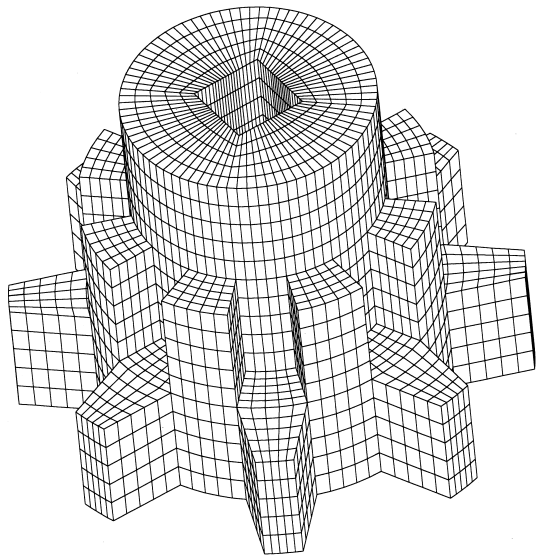

Figure 18. Numerical mesh of the gear mold.

of the square tube inserted at the center of the cylinder. Figure 19 demonstrates the shaded filling patterns at several various filling stages. This cavity developed a complex and symmetrical three-dimensional flow. The flow symmetry was accurately predicted according to Figure 19. Potential defect areas due to the multiple fronts merging are predicted, such as air entrapment, weld lines and the overflowed region. The numerical simulation model can help acquire prominent filling process information to help optimize the mold design before it is actually tooled.

Finally, it is worthwhile mentioning notice that these computations were carried out on an IBM compatible PC with 64 MB RAM and an Intel Pentium III-450 CPU. The CPU times for all of the above-presented cases were less than 30 min. Table I summarizes the number of cells, number of time steps, and memory required and CPU time of each case.

5. CONCLUSION

This work has presented an accurate three-dimensional isothermal analysis model for the injection molding. The desribed model simultaneously takes advantage of the geometrical flexibility and computational efficiency of a collocated finite volume analysis and the robustness of the algebraic volume tracking methods. Combining the FVM and the algebraic volume tracking method of the bounded compressive high resolution scheme proved a very promising solution for dealing with the polymer injection molding problems. Several illustrative examples were presented to validate the developed model and illustrate its capabilities. Comparing the

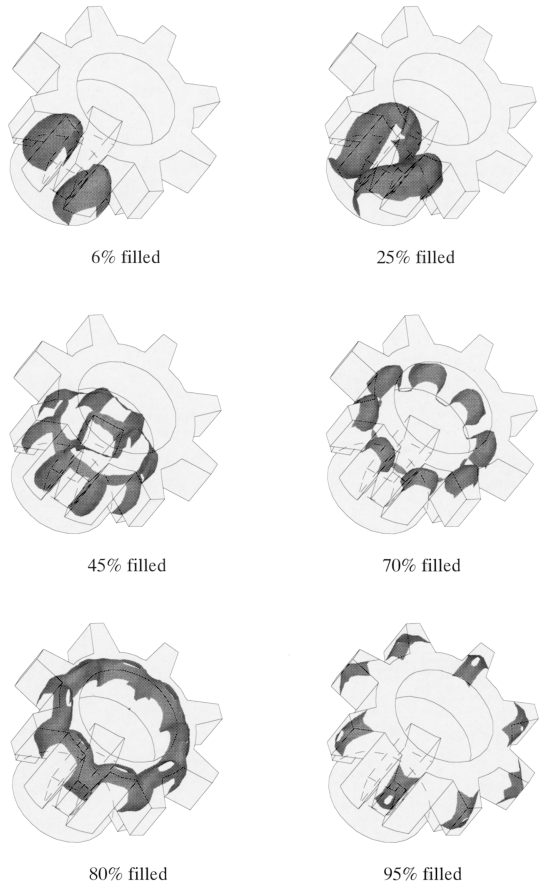

Figure 19. Simulated melt fronts at various percentages of fill.

Table I. Number of cells, number of time steps, memory and CPU times for each case (double precision is adopted)

Case	No. of CVs	No. of time steps	Memory (MB)	CPU times (s) (PIII450)
Thin plate I	5840	780	7.0	331
Thin plate II	6288	660	7.7	346
Thin plate III	8448	1200	10.7	689
Gear part	8000	1000	9.9	601

Hele–Shaw predictions and the presented three-dimensional models reveals that both models produce identical results for filling in thin cavities. Although the conventional Hele–Shaw model efficiently and accurately calculates the filling in thin cavities, the present three-

dimensional model is superior for thick cavities or cavities with a large thickness change. Moreover, the efficiency of the presented numerical model in terms of CPU time and memory requirement has maked it possible to simulate the complex three-dimensional mold filling process on a personal computer system.

The current study is limited to the isothermal, Newtonian and incompressible mold filling conditions. The extensions of the presented methodology for the non-isothermal flow of compressible non-Newtonian fluids will be reported in later publicaitons. Futhermore, the developed approach is capable of simulating other important polymer processing operations such as gas-assisted injection molding, reaction injection molding, IC packaging or multilayer coextrusion. This further research is underway.

ACKNOWLEDGMENTS

The authors would like to thank the National Science Council of the Republic of China for partially supporting this research under Contract No. NSC-89-2216-E007-018.

REFERENCES

1. Manzione LT. *Application of Computer Aided Engineering in Injection Molding*. Hanser: Munich, 1987.
2. Karmal MR, Kenig S. The injection of molding of thermoplastics, part I: theoretical model. *Polymer Engineering Science* 1972; **12**: 294–301.
3. Tadmor Z, Broyer E, Gutfinger C. Flow analysis network (FAN)—a method for solving flow problems in polymer processing. *Polymer Engineering Science* 1974; **14**: 660–665.
4. Hieber CA, Shen SF. Flow analysis of the non-isothermal two-dimensional filling process in injection molding. *Israel Journal of Technology* 1978; **16**: 248–254.
5. Stevenson JF. A simplified method for analyzing mold filling dynamics, part I: theory. *Polymer Engineering Science* 1978; **18**: 577–582.
6. Chiang HH, Hieber CA, Wang KK. A unified simulation of the filling and post-filling stages in injection molding. Part I: formulation. *Polymer Engineering Science* 1991; **31**: 116–124.
7. Kenny P. *Flow Analysis Reference Manual*. MoldFlow Pty., Ltd: Victoria, Australia, 1993.
8. Floryan JM, Rasmussen H. Numerical methods for viscous flows with moving boundaries. *Applied Mechanics Review* 1989; **12**: 323–341.
9. Harlow FH, Welch JE. Numerical calculation of time-dependent viscous incompressible flow of fluid with a free surface. *Physics of Fluids* 1965; **8**: 2182–2189.
10. Kothe DB. Perspective on Eulerian finite volume methods for incompressible interfacial flows. Technical Report LA-UR-97-3559, Los Alamos National Laboratory, 1997.
11. Hirt CW, Nichols BD. Volume of fluid (VOF) method for the dynamics of free boundaries. *Journal of Computational Physics* 1981; **39**: 201–225.
12. Minaie B, Stelson KA, Voller VR. Fluid flow and solidification modeling of die castings. *ASME Modelling of Materials Processing* 1987; **3**: 35–50.
13. Swaminathan CR, Voller VR. A time-implicit filling algorithm. *Applied Mathematical Modeling* 1994; **18**: 101–107.
14. Voller VR, Peng S. An algorithm for analysis of polymer filling of molds. *Polymer Engineering Science* 1995; **35**: 1758–1765.
15. Kim WS, Im IT. Analysis of a mold filling using an explicit SOLA-VOF. *Numerical Heat Transfer*, *Part A* 1999; **35**: 331–342.
16. Torrey MD, Mjolsness RC, Stein LR. NASA-VOF3D: a three dimensional computer program for incompressible flows with free surfaces. Technical Report LA-11009-MS, Los Alamos National Laboratory, 1987.
17. Ashgriz N, Poo JY. FLAIR: flux line-segment model for advection and interface reconstruction. *Journal of Computational Physics* 1991; **93**: 449–468.
18. Kothe DB, Mjolsness RC. RIPPLE: a new method for incompressible flows with free surfaces. *AIAA Journal* 1992; **30**: 2694–2700.
19. Lafaurie B, Nardone C, Scardovelli R, Zaleski S, Zanetti G. Modelling merging and fragmentation in multiphase flows with SURFER. *Journal of Computational Physics* 1994; **113**: 134–147.

20. Rider WA, Kothe DB. Reconstructing volume tracking. *Journal of Computational Physics* 1998; **141**: 112–152.
21. Gao DM. A three-dimensional hybrid finite element-volume tracking model for mould filling in casting processes. *International Journal for Numerical Method in Fluids* 1999; **29**: 877–895.
22. Chan KS, Pericleous KA, Cross M. Numerical simulation of flows encountered during mold filling. *Applied Mathematical Modeling* 1991; **15**: 624–631.
23. Lewis RW, Usmani AS, Cross JT. Efficient mould filling simulation in castings by an explicit finite element method. *International Journal for Numerical Methods in Fluids* 1995; **20**: 493–506.
24. Pericleous KA, Chan KS, Cross M. Free surface flow and heat-transfer in cavities—the Sea Algorithm. *Numerical Heat Transfer*, *Part B* 1995; **27**: 487–507.
25. Hetu JF, Gao DM, Garcia-Rejon A, Salloum G. 3D finite element method for the simulation of the filling stage in injection molding. *Polymer Engineering Science* 1998; **38**: 223–236.
26. Ubbink O, Issa RI. A method for capturing sharp fluid interfaces on arbitrary meshes. *Journal of Computational Physics* 1999; **153**: 26–50.
27. Patankar SV. *Numerical Heat Transfer and Fluid Flow*. McGraw-Hill: New York, 1980.
28. Ferziger JH, Peric M. *Computational Methods for Fluid Dynamics*. Springer: Heidelberg, 1996.
29. Muzaferija S. Adaptive finite volume method for flow predictions using unstructured meshes and multigrid approach. PhD thesis, University of London, 1994.
30. Davison L. A pressure correction method for unstructured meshes with arbitrary control volumes. *International Journal for Numerical Methods in Fluids* 1996; **22**: 265–281.
31. Mathur SR, Murthy JY. A pressure-based method for unstructured meshes. *Numerical Heat Transfer*, *Part B* 1997; **31**: 195–215.
32. Khosla PK, Rubin SG. A diagonally dominated second-order accurate implicit scheme. *Computer and Fluids* 1974; **2**: 207–209.
33. Saad Y. *Iterative Methods for Sparse Linear Systems*. PWS: Boston, 1996.
34. Rhie CM, Chow WL. A numerical study of the turbulent flow past an isolated airfoil with trailing edge separation. *AIAA Journal* 1983; **21**: 1525–1532.
35. Leonard BP. The ULTIMATE conservative difference scheme applied to unsteady one-dimensional advection. *Computer Methods in Applied Mechanics and Engineering* 1991; **88**: 17–74.
36. Behrens RA. Transient domain free surface flows and their applications to mold filling. PhD thesis, University of Delaware, 1983.
37. Moldex, Coretech System Co., Ltd., HsinChu, Taiwan, 1999.

